Electronic supplementary materials

for https://doi.org/10.1631/jzus.A2200334

Mechanism of the insecticidal effect of lambda-cyhalothrin loaded mesoporous silica nanoparticles with different sizes and surface modifications on *Ostrinia furnacalis* (Guenée) larvae

Yanlong WANG[1], Shuting XIAO[1], Jiang XU[1,2]✉, Daohui LIN[1,2]

[1]*Department of Environmental Science, Zhejiang University, Hangzhou 310058, China*

[2]*Zhejiang Provincial Key Laboratory of Organic Pollution Process and Control, Zhejiang University, Hangzhou 310058, China*

✉ Jiang XU, xujiang6@zju.edu.cn

Section S1 Additional details on chemicals and methods

S1.1 Chemicals

Triblock copolymer F127 (Pluronic F127, EO106PO70EO106) and hexadecyl trimethyl ammonium bromide (CTAB) were purchased from Sigma-Aldrich Chemical Co. and Macklin Biochemical (Shanghai) Co., respectively. Sodium dodecyl sulfate (SDS), tetraethyl orthosilicate (TEOS), and lambda-cyhalothrin (LCNS) standards were obtained from Aladdin Reagent Co., China. 3-Aminopropyl triethoxysilane (APTS) and chlorotrimethylsilane (TMCS) were purchased from Rhawn Reagent (Shanghai) Co. and J&K Scientific Co., Ltd., respectively. Technical LCNS (96.1% purity) was obtained from Hubei Zheng Xingyuan Chemical Co., Ltd. NaOH, KH_2PO_4, NaCl, ammonium hydroxide solution (NH_3▪H_2O), acetone, ethanol, toluene, and acetonitrile were obtained from Sinopharm Chemical Reagent (Shanghai) Co., China. All reagents and chemicals used in the experiment were of analytical reagent grade. Phosphate buffered saline (PBS) solution (pH=7.0, 25 °C) was prepared with 10 mM NaOH and 17 mM KH_2PO_4. *Ostrinia furnacalis (Guenée)* larvae and its artificial diet were provided by the Sichuan Academy of Agricultural Sciences. The purchased *O. furnacalis* larvae were bred in an artificial climate incubator (30±1 °C, 60% relative humidity, light to the dark ratio of 14 h: 10 h). Protein, ROS, superoxide dismutase (SOD), catalase (CAT), and Na^+/K^+-ATPase assay kits were purchased from the Nanjing Jiancheng Biological Engineering Company, China.

S1.2 Synthesis of bare and functionalized MSN

Mesoporous silica nanoparticle (MSN) was synthesized based on the method in our previous study (Xiao et al., 2022). CTAB and Pluronic F127 were used to direct the structure of MCN, and TEOS was used as the silica source. A mixture of TEOS, CTAB, NH_3▪H_2O, and Pluronic F127 in aqueous ethanol with a molar ratio of 2.5:0.4:50:216:1668:0.047z (z = 1–4; M_1, M_2, M_3, and M_4,

respectively) was used to prepare MSN with different sizes. The presence of hydrophobic methyl groups could improve the hydrophobicity of MSN after modification, while the modification with amino groups could change the MSN surface into positive charge due to the easy combination of amino group with hydrogen ion (Maleki et al., 2017; Suzuki et al., 2004; Yang et al., 2012). The smallest M_4 was further modified with the functional groups of -CH_3 and -NH_2 to change its surface charges and hydrophobicity. One gram of dried M_4 nanoparticles was dispersed into 100 mL toluene along with magnetic stirring (200 rpm) and nitrogen purging for 0.5 h; then, 0.5 or 1.25 mL of APTS was added followed by refluxing (110 °C, 24 h) in a nitrogen atmosphere (Liu et al., 2020; Yang et al., 2021). The obtained amino-modified M_4 nanoparticles by using 0.5 or 1.25 mL of APTS were marked as M_4–0.5NH_2 and M_4–1.25NH_2, respectively. The conditions for synthesizing methyl-modified M_4 nanoparticles were the same as the protocols for the prepared amino-modified nanocomposite, except for the use of TMCS to replace APTS and refluxing at 70 °C for 24 h (Dou et al., 2011; Jambhrunkar et al., 2014). The obtained methyl-modified nanoparticles by using TMCS with volumes of 1.25 or 2.5 mL were marked as M_4–1.25CH_3 and M_4–2.5CH_3, respectively. The specific surface area, total pore volume, and average pore diameter of each material were listed in Table S1. The size of the MSN did not significantly change their surface functional groups; –CH_3 (2930 cm^{-1}) and –CH_2– (2910 cm^{-1}) stretching vibrations (He et al., 2020) were observed on MSN with -CH_3 modification; the new bands at 1514 and 693 cm^{-1} were attributed to the in-plane and out-of-plane stretching vibrations of the amino group, suggesting the successful modification of MSN with the –NH_2 group (Fig. S1).

S1.3 Pesticide loading on bare and functionalized MCN

LCNS-loaded MSN was performed by dissolving 0.03 g of LCNS in 100 mL acetone and then dispersing MCN, M_4–NH_2, or M_4–CH_3 (0.05 g) in the solution with a 10-min sonication. The

LCNS-loaded MCN, M_4–NH_2, and M_4–CH_3 were dried under vacuum (32 °C) (Preisig et al., 2014) and marked as M/L, M_4–NH_2/L, and M_4–CH_3/L, respectively. The loading amounts of LCNS on nanoparticles were defined as the mass percentage of the total solid powders, with the percentages of M_1/L at 10.2±1.1%, M_2/L at 10.3±0.4%, M_3/L at 12.8±3.2%, M_4/L at 16.2±1.9%, M_4-0.5NH_2/L at 30.1±3.2%, M_4-1.25NH_2/L at 36.1±1.6%, M_4-1.25CH_3/L at 32.3±4.4%, and M_4-2.5CH_3/L at 71.9±11.0, respectively (Xiao et al., 2022).

S1.4 Insecticidal assessment of LCNS-loaded MSN to *O. furnacalis* larvae

Healthy third-instar larvae with a body length of about 15-20 mm were selected for the insecticidal assessment using an artificial diet-dipping assay for the combined toxicity of stomach and contact (Zhang et al., 2021a; Zhang et al., 2021b). Artificial diets dipped with LCNS-loaded MSN, LCNS, or PBS solutions were placed into a Petri dish and dried as the food for the *O. furnacalis* larvae. Artificial diets dipped with the PBS solution were used as the blank control group in this assessment. The dose transformed from the concentration of LCNS and LCNS-loaded MSN in the diet was 10 and 200 mg kg^{-1}, respectively. Ten third-instar *O. furnacalis (Guenée)* larvae with 12 h-starvation were fed with the sample-dipped artificial diet in one dish, and each experiment was replicated three times. The artificial climate incubator (BIC-800) was maintained at 30±1 °C, 60% relative humidity, light to a dark ratio of 14 h: 10 h. Larval mortality and the half-lethal dose (LD50, mg/kg) of LCNS were calculated and recorded at 24, 48, and 72 h. The environmental conditions were the same as the above protocols except for the light-to-dark ratio changing to 0 h: 24 h to analyze the effect of light on the insecticidal assessment.

S1.5 Determination of the soluble protein, ROS, antioxidase, and Na^+-K^+-ATPase activities in *O. furnacalis* larvae

O. furnacalis larvae were treated with 10 mg/kg and 200 mg/kg of LCNS and nanoparticles

(MSN, M_4/L, M_4–NH_2/L, and M_4–CH_3/L) for 6, 12, and 24 h. Three to five larvae with an insect weight of about 0.2 g were placed in a 2 mL plastic centrifuge tube, and then frozen by the liquid nitrogen. PBS buffer solution (0.01 M, pH = 7.2~7.4) was added to the plastic centrifuge tube with the ratio of insect weight (g) to buffer fluid volume (mL) being 1:9. The tissue homogenate of *O. furnacalis* larvae was prepared by mechanical homogenization (60 HZ, 1 min, and 3 times) with an ice water bath, and then by centrifugation at 2500 rpm at 4 ℃ for 10 min. The supernatant (10% tissue homogenate) was diluted 10 times with PBS buffer solution, and the contents of total protein and ROS along with the activities of SOD, CAT, and ATPase in the tissue homogenate were analyzed using the related assay kits.

Protein contents in tissue homogenate were determined by the bicinchoninic acid microplate method (Deng et al., 2013). The protein standard substance (52.4 g/L) was diluted to different concentrations with distilled water. The test or protein standard solutions with a volume of 10 μL were mixed with 250 μL bicinchoninic acid reagent with an incubation (37 ℃) for 30 min and then were analyzed by a microplate reader (Tecan infinite M200 Pro) with the absorbance at 562 nm. The protein content was calculated according to the protein standard curve with a minimum detection limit of 20 mg/L.

DCFH-DA (2, 7-Dichlorodihydrofluorescein diacetate) can be hydrolyzed to DCFH by lipoidase in cells and the DCFH can be oxidized by intracellular ROS to fluorescent DCF. Thus, the intracellular ROS contents were calculated by measuring the fluorescence intensity in the sample by using DCFH-DA as a fluorescent probe. The tissue homogenate after filtration with a 40 μm cell filter was centrifuged at 1000 g for 10 min to remove the supernatant. The treated tissue cells were suspended with 0.01 M PBS buffer solution and diluted with 10 μM DCFH-DA. The mixed solutions were incubated at 37 ℃ for 1 h, and then centrifuged at 1000 g for 10 min to remove the

supernatant. The precipitations were cleaned with buffer solution and resuspended in buffer solution. The fluorescent DCF in solution was determined using a fluorescence detector with the tested excitation/emission at 488 nm/525 nm (Hu et al., 2020).

The SOD activity in samples was determined at 450 nm by colorimetry based on water-soluble tetrazole salt (WST-1) (Yao et al., 2006). Xanthine oxidase can react with xanthine to form superoxide anion radical ($\cdot O_2^-$); WST-1 can react with $\cdot O_2^-$ to form a dirty purple dye (formazan), which could be inhibited by the reaction between SOD and $\cdot O_2^-$. Thus, the formazan content could be used to determine the inhibition rate of SOD and calculate the activity level.

The CAT activity in tissue samples was determined by a spectrophotometric method (Zhang et al., 2014). Under certain conditions, CAT can react directly with H_2O_2 in tissues, leading to the decomposition of H_2O_2. Therefore, CAT activity in tissue can be calculated by measuring the decreased absorbance of H_2O_2 at 240 nm.

ATPase can decompose ATP into ADP and inorganic phosphorus; thus, the activity of Na^+/K^+-ATPase can be quantified by measuring the content of inorganic phosphorus. The diluted 1% tissue homogenate was reacted with ATPase by water bath at 37 ℃ for 30 min; 200 μL of phosphorus standard, control, and sample solutions were taken to analyze the concentration of phosphorus; Na^+/K^+-ATPase activity was calculated based on the phosphorus content (Yao et al., 2006).

S1.6 Statistical analyses

All experiments were carried out in triplicate and the average values with standard deviations were calculated. The statistical significance of differences among treatments was evaluated by analysis of variance (ANOVA) and Duncan's multiple comparisons using SPSS Statistics 22.0 (IBM, USA), with $p < 0.05$ defined as significant.

Section S2 Additional Table and Figures

Table S1 BET surface area, total pore volume, and average pore size of MCM-48 nanoparticles with different size and functional groups. The data were adapted from our previous paper (Xiao et al., 2022)

Materials	Surface area (m^2/g)	Total pore volume (cm^3/g)	Pore size (nm)
M_1	1586	0.89	2.23
M_2	1858	0.98	2.11
M_3	1441	1.03	2.86
M_4	1634	1.46	3.56
M_4-0.5NH_2	653	0.59	2.42
M_4-1.25NH_2	389	0.40	1.48
M_4-1.25CH_3	1323	1.00	2.31
M_4-2.5CH_3	1184	0.90	2.31

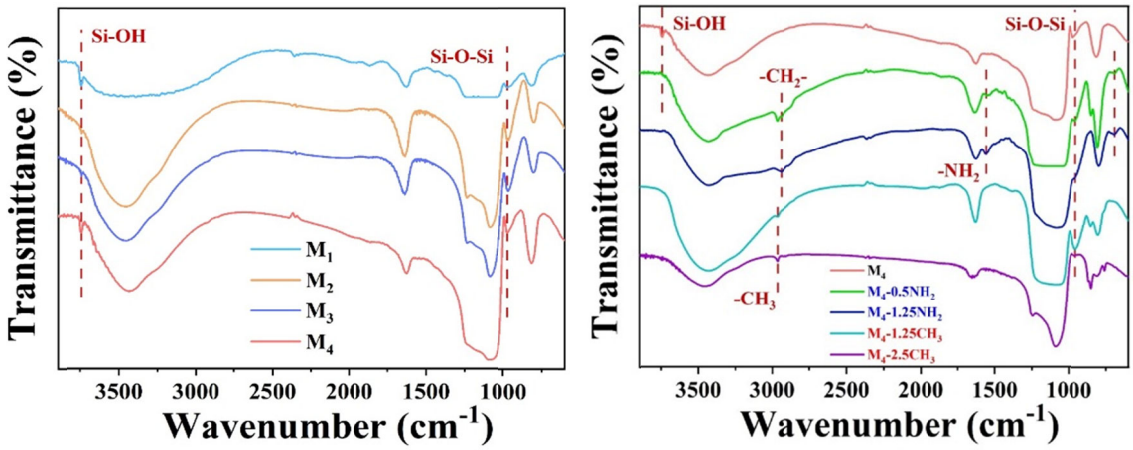

Fig. S1 (A) FTIR spectra of M_1, M_2, M_3, and M_4 obtained at 3900–600 cm^{-1}. (B) FTIR spectra obtained at 3900–600 cm^{-1} of M_4 and its functionalized versions. The data were adapted from our previous paper (Xiao et al., 2022)

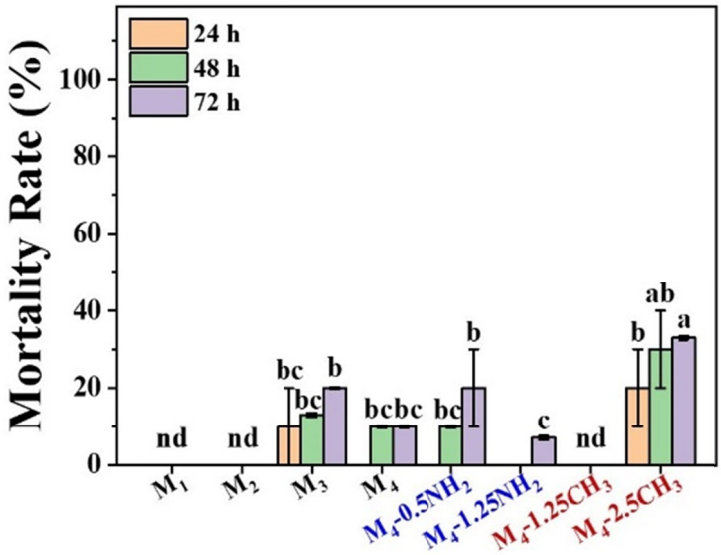

Fig. S2 The mortality rate of Ostrinia furnacalis larvae at 24, 48, 72 h after treatment by MCM-48 nanoparticles without LCNS. The data were adapted from our previous paper (Xiao et al., 2022)

References

Deng, Y., Wang, W., Yu, P., *et al.,* 2013. Comparison of taurine, GABA, Glu, and Asp as scavengers of malondialdehyde in vitro and in vivo. *Nanoscale Research Letters,* 8(1): 190-190. [doi:10.1186/1556-276X-8-190]

Dou, B.J., Hu, Q., Li, J.J., *et al.,* 2011. Adsorption performance of VOCs in ordered mesoporous silicas with different pore structures and surface chemistry. *Journal of Hazardous Materials*, 186(2-3): 1615-1624. [doi:10.1016/j.jhazmat.2010.12.051]

He, Y., Xu, H. and Liang, S. 2020. Preparation of defect-related luminescent mesoporous silica nanoparticle as potential detectable drug carrier. *Journal of Nanoscience and Nanotechnology,* 20(12): 7362-7368. [doi:10.1166/jnn.2020.18617]

Hu, C., Hou, J., Zhu, Y. and Lin, D. 2020. Multigenerational exposure to TiO_2 nanoparticles in soil stimulates stress resistance and longevity of survived *C. elegans* via activating insulin/IGF-like signaling. *Environmental Pollution,* 263: 114376. [doi:10.1016/j.envpol.2020.114376]

Jambhrunkar, S., Qu, Z., Popat, A., *et al.,* 2014. Modulating in vitro release and solubility of griseofulvin using functionalized mesoporous silica nanoparticles. *Journal of Colloid and Interface Science*, 434: 218-225. [doi:10.1016/j.jcis.2014.08.019]

Liu, Y.L., Xu, J., Cao, Z., *et al.,* 2020. Adsorption behavior and mechanism of Pb(II) and complex Cu(II) species by biowaste-derived char with amino functionalization. *Journal of Colloid and Interface Science*, 559: 215-225. [doi:10.1016/j.jcis.2019.10.035]

Maleki, A., Kettiger, H., Schoubben, A., *et al.,* 2017. Mesoporous silica materials: from physico-chemical properties to enhanced dissolution of poorly water-soluble drugs. *Journal of Controlled Release*, 262: 329–347. [doi:10.1016/j.jconrel.2017.07.047]

Preisig, D., Haid, D., Varum, F.J.O., *et al.,* 2014. Drug loading into porous calcium carbonate microparticles by solvent evaporation. *European Journal of Pharmaceutics & Biopharmaceutics*, 87(3): 548-558. [doi:10.1016/j.ejpb.2014.02.009]

Suzuki, K., Ikari, K. and Imai, H. 2004. Synthesis of silica nanoparticles having a well-ordered mesostructure using a double surfactant system. *Journal of the American Chemical Society,* 126(2): 462-463. [doi:10.1021/ja038250d]

Xiao, S.T., Shoaib, A., Xu, J., *et al.,* 2022. Mesoporous silica size, charge, and hydrophobicity affect the loading and releasing performance of lambda-cyhalothrin. *Science of the Total Environment*, 831: 154914. [doi:10.1016/j.scitotenv.2022.154914]

Yang, H., Zheng, K., Zhang, Z.M., *et al.,* 2012. Adsorption and protection of plasmid DNA on mesoporous silica nanoparticles modified with various amounts of organosilane. *Journal of Colloid and Interface Science*, 369: 317-322. [doi:10.1016/j.jcis.2011.12.043]

Yang, L.P., Kaziem, A.E., Lin, Y.G., *et al.,* 2021. Carboxylated beta-cyclodextrin anchored hollow mesoporous silica enhances insecticidal activity and reduces the toxicity of indoxacarb. *Carbohydrate Polymers*, 266: 118150. [doi:10.1016/j.carbpol.2021.118150]

Yao, X.H., Min, H. and Lv, Z.M. 2006. Response of superoxide dismutase, catalase, and ATPase activity in bacteria exposed to acetamiprid. *Biomedical and Environmental Sciences,* 19(4): 309-314.

Zhang, D.X., Du, J., Wang, R., *et al.*, 2021a. Core/shell dual-responsive nanocarriers via iron-mineralized electrostatic self-assembly for precise pesticide delivery. *Advanced Functional Materials*, 31(34): 2102027. [doi:10.1002/adfm.202102027]

Zhang, J.Q., Shen, M., Zhu, C.C., *et al.*, 2014. 3-Nitropropionic acid induces ovarian oxidative stress and impairs follicle in mouse. *Plos One*, 9(2): e86589. [doi:10.1371/journal.pone.0086589]

Zhang, Y., Fu, L., Li, S., *et al.,* 2021b. Star Polymer size, charge content, and hydrophobicity affect their leaf uptake and translocation in plants. *Environmental Science & Technology,* 55(15): 10758-10768. [doi:10.1021/acs.est.1c01065]